

# Power-Law Scaling of Structured Poly(*p*-xylylene) Films Deposited by Oblique Angle

MURAT CETINKAYA, NIRANJAN MALVADKAR, MELIK C. DEMIREL

College of Engineering, Pennsylvania State University, University Park, Pennsylvania 16802-6812

Received 30 July 2007; revised 6 November 2007; accepted 5 December 2007

DOI: 10.1002/polb.21399

Published online in Wiley InterScience (www.interscience.wiley.com).

**ABSTRACT:** This study describes the evolution and growth of structured polymers by oblique angle deposition of poly(*p*-xylylene) (PPX) derivatives. The deposition of structured PPX polymers have been demonstrated recently, but the mechanism of growth has not been studied. Here, we provide experimental evidence for the growth of structured PPX polymers by an atomic force microscope, electron microscope, and a profilometer. Individual columns expand with respect to their heights according to a power-law,  $d = ch^p$ , where  $d$  is the column diameter,  $c$  and  $p$  are constants, and  $h$  is the height of a column. Values of  $p$  for structured poly(chloro-*p*-xylylene), poly(trifluoroacetyl-*p*-xylylene-*co-p*-xylylene), and poly(bromo-*p*-xylylene) films are estimated as  $0.11 \pm 0.01$ ,  $0.15 \pm 0.01$ , and  $0.18 \pm 0.01$ , respectively. This result is different from the traditional oblique angle deposition processes of nonpolymeric materials where the surface diffusion is low. Further analysis with two-dimensional power spectral density (PSD) method showed that the ordering of columns is quasi-periodic. Additionally, the X-ray and transmission electron microscope characterization of the columns revealed that the columns are semicrystalline. © 2008 Wiley Periodicals, Inc. *J Polym Sci Part B: Polym Phys* 46: 640–648, 2008

**Keywords:** growth; nanotechnology; poly(*p*-xylylene); scaling; self-organization; structured polymers; thin films

## INTRODUCTION

The growth of spatially organized structures is of considerable fundamental interest, since it may provide us with important clues to the way in which organized structures form in Nature. A closer look at complex structures in insect wings and lizard toes reveal organized structured features at the microscopic scale. Recent studies on gecko footpads showed that the attractive forces that hold geckos to surfaces are van der Waals interactions between the finely divided keratinous fibers (500,000 on each foot) and the surfaces themselves.<sup>1–3</sup> Similarly, outermost portion

of the exoskeleton of an insect wing has organized nanometer scale structures (densely covered features that are on average 150 nm in diameter) which serve many functions in defense and display.<sup>4,5</sup> The organized structures in Nature are formed through evolutionary processes, and these complex molecules and features are built using molecular protein machinery. These structured biological polymers (or structured proteins) have amorphous and crystalline regions, which exhibit long-range order at the nanometer scale.

Synthetic polymers, that mimic biological materials in their designs, form organized structures too.<sup>6</sup> Recently, we showed that structured polymers can be fabricated by an oblique angle deposition method.<sup>7–11</sup> These structures are composed of ~40,000,000 aligned columns (~150 nm in diameter) per square millimeter

Correspondence to: M. C. Demirel (E-mail: mdemirel@engr.psu.edu)

*Journal of Polymer Science: Part B: Polymer Physics*, Vol. 46, 640–648 (2008)  
© 2008 Wiley Periodicals, Inc.

similar to the gecko footpad or insect wing. The structured polymer formation is a bottom-up approach and the production technique does not require any template or lithography method or a surfactant for deposition.<sup>7–11</sup>

Growth by oblique angle deposition for nonpolymeric materials (e.g., silicon, tungsten, copper, and gold) have been studied extensively.<sup>12–15</sup> However, the study of nucleation and growth for polymers by oblique angle method has not been reported. In general, nucleation and growth (common in these films<sup>16,17</sup>), geometric shadowing,<sup>15</sup> and columnar growth leading to oriented crystallization<sup>12</sup> are the variables that influence the formation of structured films. Because of geometric shadowing and competitive growth phenomena, isolated columns emerge on the substrate.<sup>12</sup>

In this article, the nucleation and growth of three structured poly(*p*-xylylene) (PPX) derivatives are studied. Characterization of structured PPX films is performed with an atomic force microscope (AFM), transmission electron microscope (TEM), and grazing X-ray analysis. Different stages of columnar growth as a function of column diameter are characterized by AFM. Two-dimensional power spectral density (PSD) method is adopted for revealing the quasi-periodicity of surface features at certain stages of columnar growth.

An understanding of ways to control nucleation as well as growth of structured polymers would be beneficial, not only in advancing the state of knowledge in the area of polymers, but also because of the potential impact that this information would have on the development of new materials for antifouling surfaces, catalyst supports, medical implants, optical devices, and sensor platforms. The structured polymers offer the possibility of fabricating surfaces exhibiting tunable properties (e.g., hydrophobicity, electrochemistry, chemical reactivity, and surface energy) by systematically varying and controlling the surface chemistry and morphology at the same time.

## EXPERIMENTAL

### Oblique Angle Deposition

The deposition of structured PPX polymer films by vapor deposition<sup>18</sup> is performed as previously described.<sup>7–11</sup> Briefly, deposition of a structured PPX-derivative film starts with [2.2]paracyclophane (Fig. 1), which is placed in a vacuum chamber and converted to a reactive gas of monomers by pyrolysis (600–690 °C). The substrates are cleaned with acetone and isopropanol, and dried with nitrogen. The substrate is

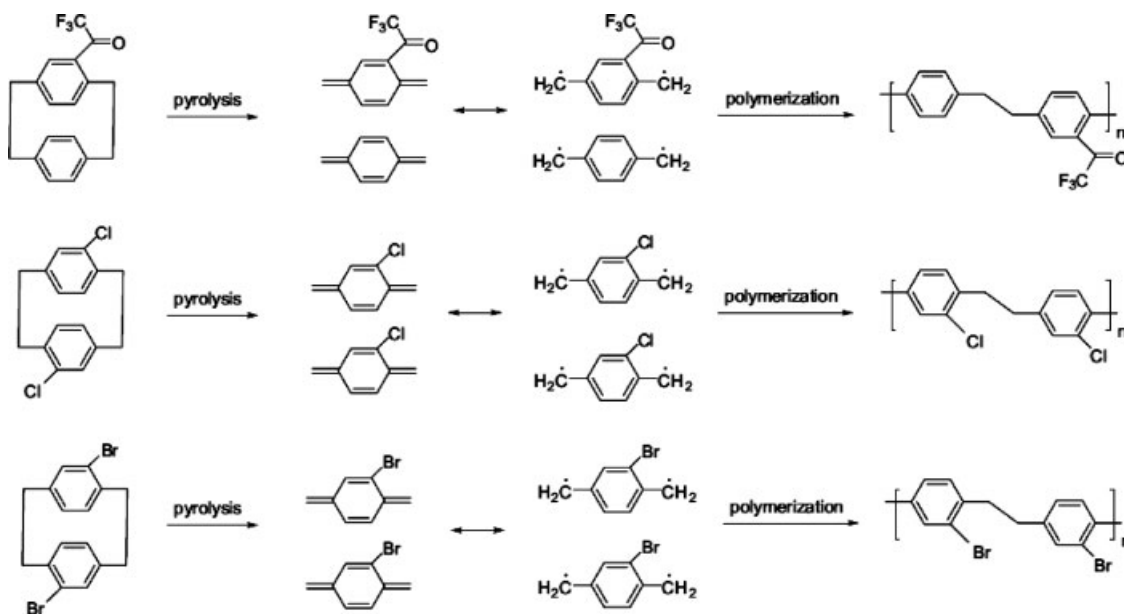


**Figure 1.** Polymerization of poly(*o*-chloro-*p*-xylylene) (PPX-Cl), poly(*o*-bromo-*p*-xylylene) (PPX-Br), and poly(*o*-trifluoroacetyl-*p*-xylylene-co-*p*-xylylene) (PPX-COCF<sub>3</sub>) are shown.

held fixed in a tilted orientation relative to the incoming vapor ( $10^\circ$  between substrate and nozzle). The vapor pressure in deposition chamber is maintained at  $\sim 30$ – $50$  mbar. Deposition process is completed in 10 min after the required vacuum level has been achieved.

### Film Characterization

Synthesis of paracyclophane derivatives (PPX-COCF<sub>3</sub>, poly(trifluoroacetyl-*p*-xylylene-*co-p*-xylylene), PPX-Br, (poly(bromo-*p*-xylylene)), and PPX-Cl, poly(chloro-*p*-xylylene)) PPX films are previously described.<sup>8–10</sup> All surface measurements are performed with a Nanoscope-E atomic force microscope (AFM) (Veeco Metrology, CA). Topography images are collected in ambient air at room temperature, with silicon nitride (SiN) triangular cantilevers having contact mode tips (DNP Series,  $k = 0.58$  N/m, Veeco Metrology, CA). Film thickness (i.e., column height) is measured with a Tencor P10 profilometer. Scanning parameters for the profilometer are as follows: scan speed is  $20 \mu\text{m/s}$ , stylus force is 1 mg, and sampling rate is 200 Hz.

### Crystallinity

X-ray diffractions (XRD) are performed with a Scintag X2 X-ray diffractometer with a Cu K $\alpha$  radiation source. X-ray pattern is obtained with an angle step of  $0.02^\circ$  and 1.5 s waiting time between each step. Percent crystallinity is calculated by taking the ratio of areas under crystalline peaks in a pattern to the total area under the pattern. Electron diffraction pattern was obtained using a Philips-420 tungsten-based TEM operating at 120 kV. Sections of 80–100 nm thicknesses were taken using a Leica Ultracut UCT Microtome at cryogenic conditions. These sections were taken parallel to the direction of the flux and perpendicular to the film surface. Cut sections were placed on a carbon coated copper grid and then imaged using the TEM.

### Data Acquisition and Preparation

AFM topography images are acquired with Nanoscope Software (Veeco Metrology, CA). Each measurement is replicated three times and averaged results are presented. AFM topography images are modified with the “highpass” tool of Nanoscope Software prior to further analysis. Highpass calculates the weighted difference between a pixel in the image and its eight neighbors. This data point is then replaced by the calculated difference. This operation is beneficial in highlighting edges of the columns. Image quality is kept at  $256 \times 256$  pixels.

### Data Analysis

To generate input for the PSD function and column diameter calculations, column boundaries are located from the recorded AFM images. Two-dimensional PSD calculations are completed with Nanoscope Software using  $5 \mu\text{m}$  scans. Column sizes are calculated with ImageJ using  $2 \mu\text{m}$  scans.<sup>19</sup> Threshold adjustment is applied to  $2 \mu\text{m}$  scans for column detection, where the column edges are identified automatically (Table 1). We also repeated the column diameter measurement manually. There are variations in the manually calculated values of column diameters with that of the software calculations because of inaccuracy of edge detection. Small surface features or experimental noise appear at the high frequency regions of the PSD plots. On the other hand, surface defects appear at the low frequencies.

## RESULTS

We studied the evolution and growth of structured poly(chloro-*p*-xylylene) (PPX-Cl), poly(bromo-*p*-xylylene) (PPX-Br), and poly(trifluoroacetyl-*p*-xylylene-*co-p*-xylylene) (PPX-COCF<sub>3</sub>) films by oblique angle deposition. (Fig. 1) Structured PPX films are deposited on a substrate from a directional vapor source of reactive vapor of monomers in a vacuum chamber. The substrate is oriented obliquely relative to the vapor flux, at an angle

**Table 1.** Calculated Values of  $c$  and  $p$  Constants in eq 1

Type	$c$	$p$	$c$ (manual)	$p$ (manual)
PPX-COCF <sub>3</sub>	$47.68 \pm 4.00$	$0.15 \pm 0.01$	$96.75 \pm 26.97$	$0.11 \pm 0.04$
PPX-Cl	$55.20 \pm 2.23$	$0.11 \pm 0.01$	$92.21 \pm 1.82$	$0.08 \pm 0.00$
PPX-Br	$37.92 \pm 1.84$	$0.18 \pm 0.01$	$50.76 \pm 11.67$	$0.18 \pm 0.03$

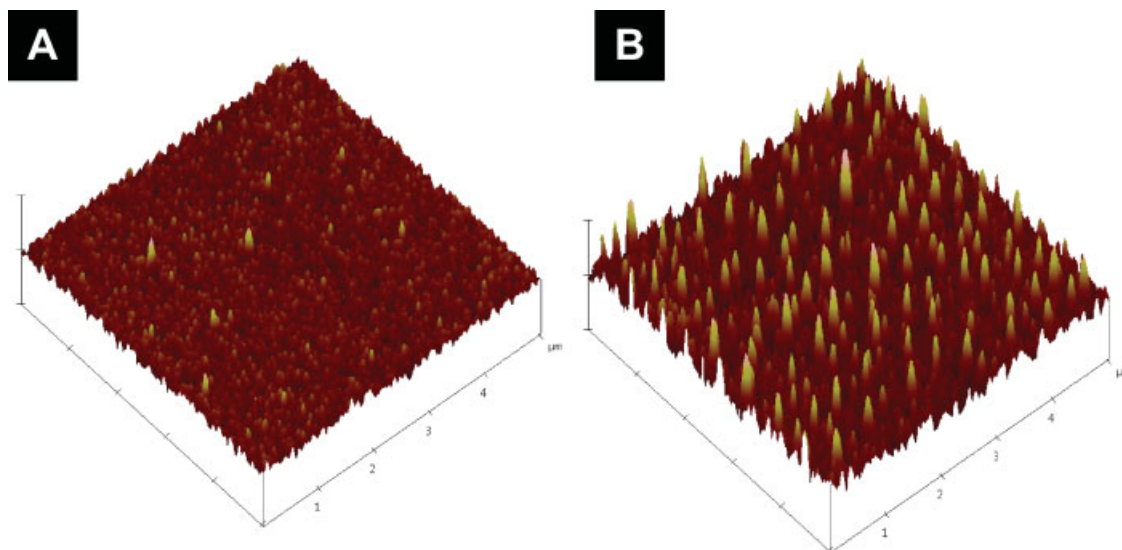


**Figure 2.** AFM images of early stage roughness (A) and columnar growth (B) due to oblique-angle deposition processes (scale bars for the AFM scan: X:1  $\mu\text{m}/\text{div}$ , Y:1  $\mu\text{m}/\text{div}$ , Z:50 nm/div). The structured poly(*p*-xylylene) film is deposited on a substrate at an oblique angle ( $\alpha = 10^\circ$ ).

$\alpha = 10^\circ$ , which creates a porous and low-density film of columns inclined at an angle  $\phi \geq \alpha$ . Oblique angle deposition of PPX yields isolated slanted columns. Initial stages of columnar growth are characterized with atomic force microscopy. AFM images during the deposition of a PPX film show the step by step evolution of columnar morphology. Figure 2(A) shows that a rough thin film ( $\sim 1\text{--}5$  nm RMS roughness) forms on the substrate. Figure 2(B) shows that columns start to grow toward incoming vapor, and the areas in between columns are shadowed due to an oblique angle deposition.

Characterization of PPX-Cl, PPX-Br, and PPX-COCF<sub>3</sub> revealed a growth mechanism obeying the power-law scaling. Power-law scaling proposes a columnar growth by relating its diameter to its height with an allometric equation as follows:

$$d = ch^p \quad (1)$$

where  $d$  is the column diameter,  $c$  and  $p$  are constants, and  $h$  is the height of a column. Figure 3 shows data points and corresponding best fits for column width with respect to column heights for three PPX derivatives. A single exponent,  $p$ , is employed in eq 1 due to the isotropy of the columns. In other words, column size can be parameterized with a single, direction independent parameter, which is the column diame-

ter. Film thickness is measured by a profilometer and the column height is the film thickness divided by the sinus of the slanting angle,  $\phi$ , of the columns.

Values of  $p$  for PPX-Cl, PPX-COCF<sub>3</sub>, and PPX-Br films are estimated as  $0.11 \pm 0.01$ ,  $0.15 \pm 0.01$ , and  $0.18 \pm 0.01$ , respectively (Table 1).

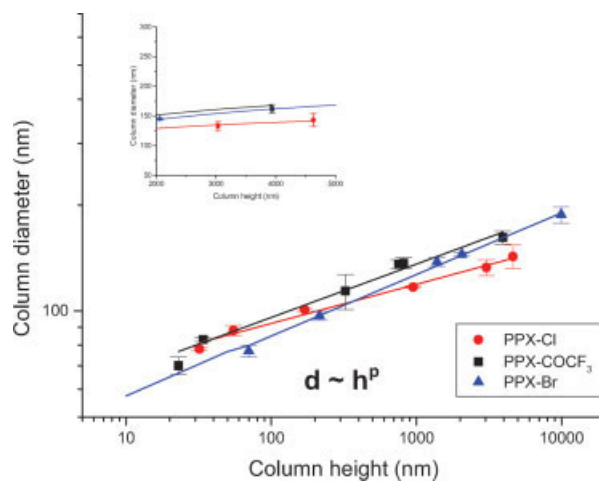


**Figure 3.** Power-law growth ( $d \sim h^p$ , where  $d$  is the column diameter and  $h$  is the column height) is observed in columnar growth for structured PPX-Cl, PPX-Br, and PPX-COCF<sub>3</sub> films. Error bars represent the standard deviations based on three sets of measurements. The inset shows convergence of column diameter as a function of height for all three films.

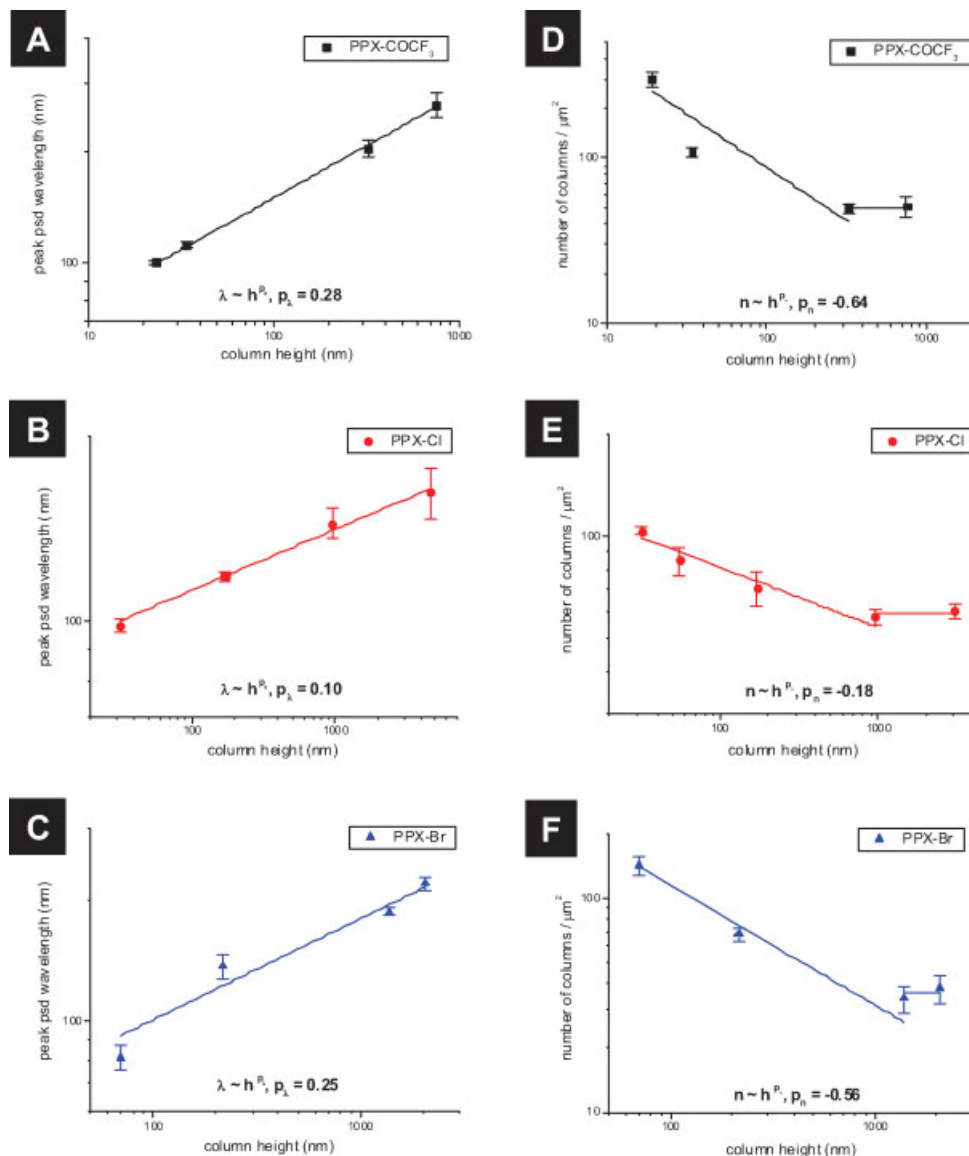


**Figure 4.** Peak PSD wavelength and number of columns per unit area as a function of column height plots for PPX-COCF<sub>3</sub> (A,D), PPX-Cl (B,E), and PPX-Br (C,F) films are shown. Solid lines represent the best fits and error bars are the deviations based on three measurements. [Color figure can be viewed in the online issue, which is available at [www.interscience.wiley.com](http://www.interscience.wiley.com).]

A smaller exponent for PPX-Cl film shows that columns grow faster than the other two films. Karabacak et al.<sup>13,21</sup> calculated that the exponent  $p$  values below 0.31 are associated with diffusion according to Mullins-Herring model.<sup>22,23</sup> Therefore, our  $p$  values are in the diffusion range. Although the exact dependence between surface diffusion and columnar growth is unknown for polymeric materials, it can be

inferred that PPX-Cl monomers experience a higher surface diffusion compared to the PPX-Br and PPX-COCF<sub>3</sub> monomers.

We also investigated the periodicity for structured PPX films. The variation in periodicity is compared for different stages of columnar growth. Periodicity of the columns is measured by PSD method. Two-dimensional PSD function is defined as:

**Table 2.** Calculated Values of  $c_n$ ,  $p_n$ ,  $c_\lambda$ , and  $p_\lambda$  Constants in eq 3

Type	$c_n$	$p_n$	$c_\lambda$	$p_\lambda$
PPX-COCF <sub>3</sub>	1699.24 ± 313.11	-0.64 ± 0.01	41.80 ± 2.05	0.28 ± 0.01
PPX-Cl	182.59 ± 29.04	-0.18 ± 0.04	71.04 ± 3.64	0.10 ± 0.01
PPX-Br	1515.12 ± 718.81	-0.56 ± 0.10	31.83 ± 9.21	0.25 ± 0.04

$$\text{PSD} = \frac{1}{A} \left| \frac{1}{2\pi} \int dx \int dy e^{i(px+qy)} h(x,y) dy \right|^2 \quad (2)$$

where,  $h(x, y)$  is the height at location  $(x, y)$ ,  $p$  and  $q$  are frequencies in  $x$  and  $y$  directions, and  $A$  is the scanned area. Here, PSD is a function of lateral frequencies  $p$  and  $q$ , and the integrations are done over all data points  $(x, y)$  on the surface. If the surface is isotropic, a single frequency  $k = [p^2 + q^2]^{1/2}$  can be evaluated in PSD function. Peak PSD frequency ( $k_{\max}$ ) and the corresponding peak wavelength ( $\lambda = 2\pi/k_{\max}$ ) are estimated by fitting a Gaussian curve to PSD data. PSD provides both lateral and vertical information about surface features, and yields the relative weight of a column roughness with respect to its spatial frequency.<sup>24</sup> AFM scans (1, 2, and 5  $\mu\text{m}$ ) are performed to cover a sufficiently large spatial frequency and to ensure consistency between results from different scan sizes. Figure 4(A–C) represent the results from 5  $\mu\text{m}$  AFM scans for the peak PSD wavelength as a function of column height of PPX-COCF<sub>3</sub>, PPX-Cl, and PPX-Br, respectively. This data also implies the existence of lateral periodicity in columnar morphology of structured PPX films. Figure 4(D–F) represent the number of columns as a function of column height. A power-law scaling between the column height, PSD wavelength, and number of columns also exist.

$$\begin{aligned} n &= c_n h^{p_n} \\ \lambda &= c_\lambda h^{p_\lambda} \end{aligned} \quad (3)$$

where  $n$  is the number of columns, and  $\lambda$  is the peak PSD wavelength at height  $h$ . We note that the exponent  $p_\lambda$  can be correlated to  $p_n$  by using a relationship between the column number density and the wavelength. Theoretically, substitution of the first power law into the second one in eq 3 should give  $p_\lambda = -1/2 p_n$  (i.e., assuming  $\lambda^2 \sim 1/n$ ). Our experimental values for the  $p_\lambda/p_n$  ratio are -0.44, -0.55, and -0.45 for PPX-

COCF<sub>3</sub>, PPX-Cl, and PPX-Br films, respectively (Table 2). The experimental results are in good agreement with the theoretically predicted power ratio  $p_\lambda/p_n (= -0.5)$ .

Figure 4(D–F) show that columns continue to expand until a critical film thickness is achieved. PPX columns expand as they grow

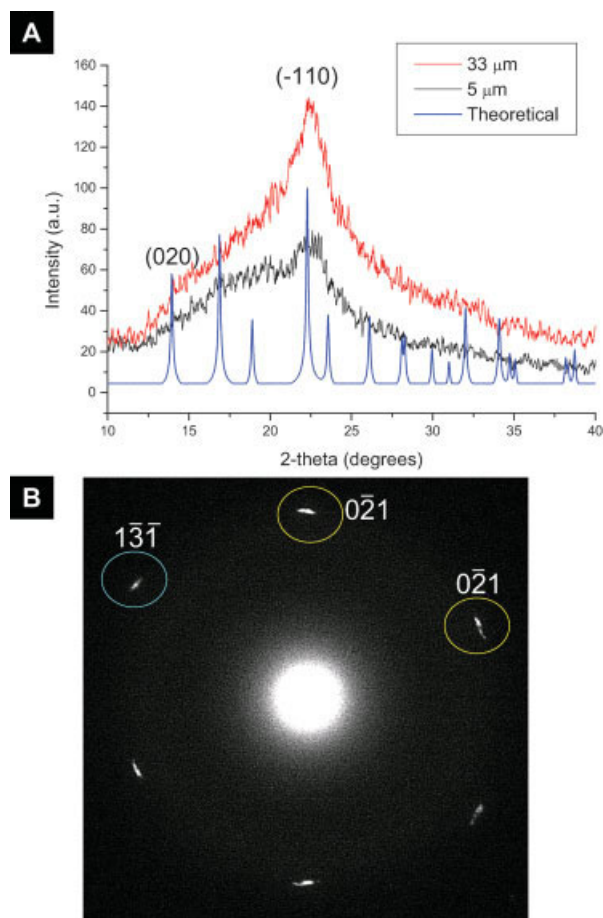


**Figure 5.** (A) X-ray diffraction pattern of PPX-Cl films of various thicknesses. Theoretical peaks for  $\alpha$ -phase are shown with dashed lines. (B) Electron diffraction pattern of PPX-Cl film and corresponding crystalline indices are shown. [Color figure can be viewed in the online issue, which is available at [www.interscience.wiley.com](http://www.interscience.wiley.com).]

during the initial deposition process. Consequently, columnar expansion leads to a competitive growth due to increasing shadowed areas and thus the number of surviving columns decrease as the column height increases. Column diameter saturates after the critical thickness is reached where the number of columns do not change. The critical film thicknesses for the PPX-Br and PPX-Cl films are  $\sim 1 \mu\text{m}$ , and PPX-COCF<sub>3</sub> film is  $\sim 400 \text{ nm}$ . The PPX-COCF<sub>3</sub> is grown at a higher vapor pressure (i.e., faster growth rate in both vertical and lateral directions) than the other two films. Therefore, we expect that it would reach the critical film thickness at a lower value than the other two films.

We studied the crystallinity of the PPX-Cl film by grazing X-ray analysis and TEM. It is known that PPX possesses a crystalline morphology when deposited by the vapor deposition technique.<sup>18</sup> The PPX crystallites tend to be mostly of the  $\alpha$ -phase and are confined to small nanometer domains that are randomly dispersed throughout an amorphous continuum. The measured XRD pattern in Figure 5(A) shows that structured PPX films are semicrystalline  $\alpha$  form. Two columnar PPX-Cl films with different

thickness are deposited under identical conditions. The thinner one is around  $5 \mu\text{m}$  thick, whereas the thicker one is  $33 \mu\text{m}$ . Their XRD patterns are obtained under identical conditions (see experimental section). A major peak, (1, -1, 0), is identified from the XRD data. Both films are typically about 30% crystalline. Figure 5(B) shows the electron diffraction pattern of PPX-Cl columns that are obtained from cross sectional TEM analysis. The columns have crystalline regions defined by  $\alpha$ -phase. The diffraction pattern of PPX-Cl is also calculated using the Mercury Software<sup>25</sup> based on a monoclinic unit cell with  $a = 596 \text{ pm}$ ,  $b = 1269 \text{ pm}$ ,  $c$  (chain axis) =  $666 \text{ pm}$ ,  $\beta = 135.2^\circ$ .<sup>26</sup> Two major peaks, (0, -2, 1) and (1, -3, -1), are identified from the electron diffraction data.

## DISCUSSION

Film growth models by oblique angle deposition have been studied by atomic scale simulations such methods as Monte Carlo and molecular dynamics.<sup>27,28</sup> These models combine atomistic ballistic deposition with a kinetic Monte Carlo algorithm for surface diffusion. In general, the

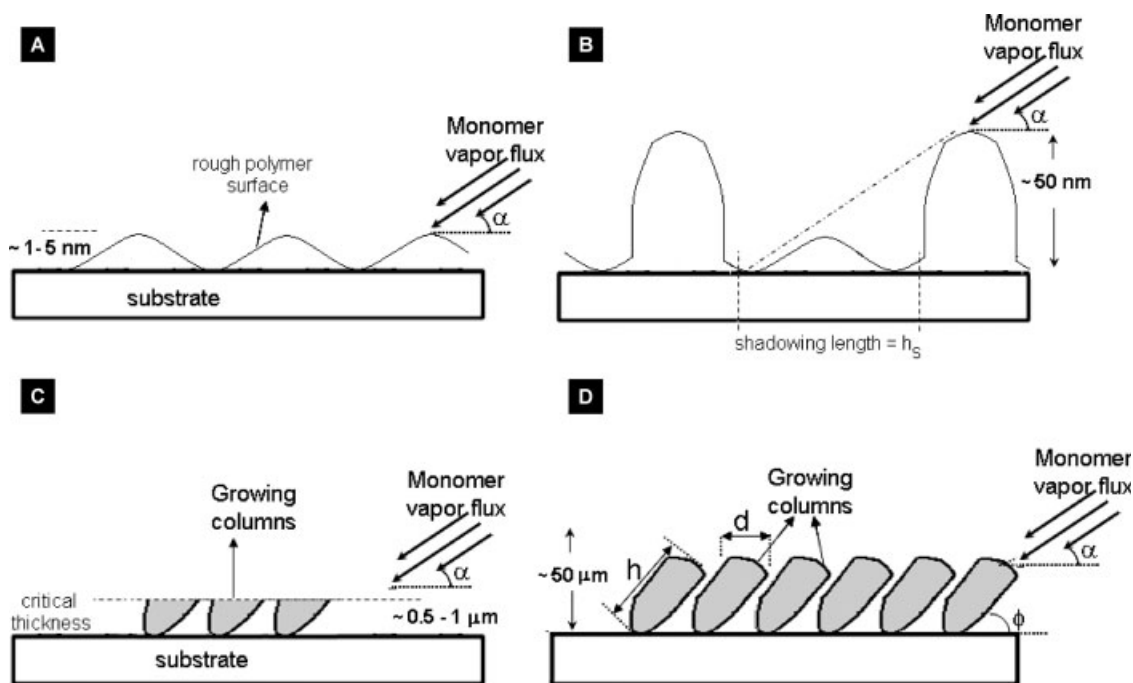


**Figure 6.** Schematic of growth model for columnar PPX films. (A) Early stage roughness, (B) geometric shadowing and column growth, (C) column expansion before critical film thickness, and (D) growth after critical film thickness are shown.

models suggest an initial exponential growth of columns and a uniform growth after a critical thickness. The models are consistent with the experimental observations on the structural growth, such as porosity depth profile and scaling growth.

We also observed a scaling growth mechanism for our polymer films. Our model includes three steps. First, a thin PPX film grows on a smooth surface [Fig. 6(A)]. At this early stage, surface roughness is destabilized by a geometric shadowing process. The vapor flux arrives at an oblique angle that leads to formation of higher surface features due to geometric shadowing process. The higher surface features (columns) shadow a nearby region of lower surface heights [Fig. 6(B)]. All of the incident monomers that approach this region are captured by the columns. To fill shadowed length between columns, incoming monomers must undergo very large number of hops. Shadowing length can be calculated from simple geometric consideration as  $h_s = h/\tan(\alpha)$ . For example, the columns are 50 nm tall in Figure 2(B) and corresponding shadowing length [ $50/\tan(10)$ ] is 250 nm, which agrees well with separation of columns in Figure 2(B).

Second, as the film gets thicker, columns get wider [Fig. 6(C)]. Diffusion on the column surface, and flux rate affect this step. We observed that the growth is faster ( $\sim 50$ – $100$  nm/s) in these films compared to the growth of nonpolymeric materials. This is due to high surface diffusion on polymer films. The surface diffusion of PPX monomers should be high in contrast to traditional oblique angle deposition processes because the polymerization reaction occurs only at the ends of a polymer chain.<sup>29</sup> The reactive monomer has to search the end of the polymer after it is condensed on the substrate.<sup>18</sup> We also note that the power-law exponent,  $p$ , depends not only on the existence of surface diffusion and self-shadowing process, but also on deposited material and deposition angle. This has been reported in a detailed study by Buzea et al.<sup>30</sup> for nonpolymeric materials.

Finally, the number of columns decreases as the film gets thicker until a critical thickness is reached. The columns then start to grow uniformly [Fig. 6(D)] after the critical thickness ( $\sim 1$   $\mu\text{m}$ ). All three films have approximately very similar number of columns per square micron area (40, 50, and 60 for PPX-Br, PPX-COCF<sub>3</sub>, and PPX-Cl, respectively). The average

distance between columns is estimated as  $\sim 250$  nm from the peak PSD wavelength data, and is consistent with the shadowing length ( $\sim 250$  nm).

## CONCLUSIONS

This study shows that oblique angle deposition of PPX derivatives creates structured polymers with the following characteristics: (i) At the early stage of the growth the roughness on the surface is affected by an incoming oblique vapor deposition. The random differences in the height of surface features induce columnar growth due to shadowing. (ii) Growth of PPX columns obeys a power-law scaling mechanism. The power-law exponent,  $p$ , in eq 1 shows the rate of expansion of columns deposited by oblique angle. Comparison of  $p$  values for PPX-Cl, PPX-Br, and PPX-COCF<sub>3</sub> indicate that high surface diffusion and high flux of incoming vapor molecules is a major factor affecting the columnar formation. (iii) PSD analysis showed that PPX columns are quasi-periodically segregated on a surface. Periodicity of the surface varies during the initial growth of the columns, but converges after a certain film thickness ( $\sim 1$   $\mu\text{m}$ ) is achieved. (iv) The XRD and TEM characterization of the columns revealed that the columns are semi-crystalline.

Significant opportunities exist for further improvement of the model to understand the structured polymer deposition by oblique angle deposition. Specifically, the model could be extended to incorporate the effects of polymerization and crystallinity. Understanding the growth and formation of structured polymers will represent significant progress toward the development of new three-dimensional functionalized surfaces for medical and engineering applications. Our future work will focus on understand of the effect of these parameters on the columnar growth of polymers by oblique angle deposition.

This research is supported by a Young Investigator Program Award from the Office of Naval Research (N000140710801).

## REFERENCES AND NOTES

1. Huber, G.; Mantz, H.; Spolenak, R.; Mecke, K.; Jacobs, K.; Gorb, S. N.; Arzt, E. *Proc Natl Acad Sci USA* 2005, 102, 16293–16296.

2. Autumn, K.; Sitti, M.; Liang, Y. C. A.; Peattie, A. M.; Hansen, W. R.; Sponberg, S.; Kenny, T. W.; Fearing, R.; Israelachvili, J. N.; Full, R. J. *Proc Natl Acad Sci USA* 2002, 99, 12252–12256.
3. Ruibal, R.; Ernst, V. *J Morphol* 1965, 117, 271–275.
4. Wootton, R. J. *Annu Rev Entomol* 1992, 37, 113–140.
5. Vincent, J. F. V.; Wegst, U. G. K. *Arthropod Struct Dev* 2004, 33, 187–199.
6. Forster, S.; Plantenberg, T. *Angew Chem Int Ed* 2002, 41, 689–714.
7. Boduroglu, S.; Cetinkaya, M.; Dressick, W. J.; Singh, A.; Demirel, M. C. *Langmuir* 2007, 23, 11391–11395.
8. Demirel, M. C.; Boduroglu, S.; Cetinkaya, M.; Lakhtakia, A. *Langmuir* 2007, 23, 5861–5863.
9. Cetinkaya, M.; Boduroglu, S.; Demirel, M. C. *Polymer* 2007, 48, 4130–4134.
10. Pursel, S.; Horn, M. W.; Demirel, M. C.; Lakhtakia, A. *Polymer* 2005, 46, 9544–9548.
11. Demirel, M. C.; So, E.; Ritty, T. M.; Naidu, S.; Lakhtakia, A. *J Biomed Mater Res B* 2007, 81B, 219–223.
12. Young, N. O.; Kowal, J. *Nature* 1959, 183, 104–105.
13. Karabacak, T.; Singh, J. P.; Zhao, Y. P.; Wang, G. C.; Lu, T. M. *Phys Rev B* 2003, 68, Art. No. 125408.
14. Martin-Palma, R. J.; Ryan, J. V.; Pantano, C. G. *J Appl Phys* 2007, 101, Art. No. 083513.
15. Hawkeye, M. M.; Brett, M. J. *J Vac Sci Technol A* 2007, 25, 1317–1335.
16. Kuprat, A.; George, D.; Straub, G.; Demirel, M. C. *Comput Mater Sci* 2003, 28, 199–208.
17. Demirel, M. C.; Kuprat, A. P.; George, D. C.; Straub, G. K.; Rollett, A. D. *Interface Sci* 2002, 10, 137–141.
18. Gorham, W. F. *J Polym Sci Part A-1: Polym Chem* 1966, 4, 3027–3039.
19. Abramoff, M. D.; Magelhaes, P. J.; Ram, S. J. *Biophotonics Intl* 2004, 11(7), 36–42.
20. Beydaghyan, G.; Kaminska, K.; Brown, T.; Robbie, K. *Appl Opt* 2004, 43, 5343–5349.
21. Karabacak, T.; Wang, G. C.; Lu, T. M. *J Appl Phys* 2003, 94, 7723–7728.
22. Mullins, W. W. *J Appl Phys* 1957, 28, 333–339.
23. Herring, C. *J Appl Phys* 1950, 21, 301–303.
24. Fang, S. J.; Haplepete, S.; Chen, W.; Helms, C. R.; Edwards, H. *J Appl Phys* 1997, 82, 5891–5898.
25. Mercury. The Cambridge Crystallographic Data Centre: Cambridge, 2004.
26. Iwamoto, R.; Wunderli, B. *J Polym Sci Part B: Polym Phys* 1973, 11, 2403–2411.
27. Dong, L.; Smith, R. W.; Srolovitz, D. J. *J Appl Phys* 1996, 80, 5682–5690.
28. Meakin, P.; Krug, J. *Phys Rev A* 1992, 46, 3390–3399.
29. Zhao, Y. P.; Fortin, J. B.; Bonvallet, G.; Wang, G. C.; Lu, T. M. *Phys Rev Lett* 2000, 85, 3229–3232.
30. Buzea, C.; Beydaghyan, G.; Elliott, C.; Robbie, K. *Nanotechnology* 2005, 16, 1986–1992.